



Sintered diamond as a hybrid EDM and grinding tool for the micromachining of single-crystal SiC

Jiwang Yan (2)*, Tsong-Han Tan

Department of Mechanical Engineering, Keio University, Yokohama 223-8522, Japan



ARTICLE INFO

Keywords:
Electrical discharge machining
Grinding
Sintered diamond

ABSTRACT

Sintered diamond was used as a hybrid tool for micro-scale electrical discharge machining (EDM) and grinding of single-crystal SiC to achieve both high efficiency and surface integrity. Material removal behavior, surface topography, and subsurface damage for both process steps were investigated under various conditions. The results showed that SiC decomposed into Si and C during EDM, creating a very thick recast layer which had remarkably lower hardness than the bulk. Owing to the electrical dressing effect in EDM, diamond grains protrude out of tool surface and grind the recast layer in a ductile manner with low tool wear. An extremely smooth surface ($R_a = 1.85 \text{ nm}$) was obtained.

© 2015 CIRP.

1. Introduction

Single-crystal silicon carbide (SiC) is an excellent material for high-temperature and high-power electronic devices and micro-electro-mechanical systems (MEMS). Compared to Si, SiC has higher thermal conductivity, current density, and breakdown electric field strength, as well as a broader band gap. However, owing to its hardness and brittleness, SiC is very difficult to machine [1]. Currently, SiC is finished by chemomechanical polishing (CMP), but the material removal rate (MRR) is extremely low. On the other hand, SiC is electrically conductive, meaning it can be finished by electrical discharge machining (EDM) [2–4], which has a much higher MRR.

In this study, we attempted the EDM of SiC using sintered diamond (polycrystalline diamond, PCD) as a tool electrode. After EDM shaping, the same PCD tool was used to grind the electrical discharge machined (EDMed) surface and to remove both the subsurface damage and recast layer formed during EDM. The proposed process was demonstrated to enable high-efficiency, high-precision, and low-damage micromachining of SiC. The mechanisms for surface formation, structural changes of material, and tool wear in the two-step machining process were investigated by Raman spectroscopy and cross-sectional scanning electron microscopic (SEM) observation. Optimal conditions for both process steps were experimentally explored.

2. Scheme of PCD hybrid tool

PCD is a composite of diamond grains sintered with a metallic binder such as Co. PCD is not only excellent for cutting and milling [5–8], but also useable as an electrode for EDM. It has been demonstrated that in EDM of tungsten carbide and die steel, the wear of PCD electrodes is extremely low due to its high thermal

conductivity and high melting point [9,10]. In this study, we attempt the EDM of SiC using PCD electrodes to realize a higher MRR of SiC and a lower electrode wear rate than when using other electrode materials such as Cu and W [2–4]. EDM typically creates high surface roughness and severe subsurface damage (SSD) including microcracks and material phase changes, as illustrated in Fig. 1a. Although the SSD layer can be removed by special polishing processes, such as plasma-assisted polishing [11], such polishing is very time-consuming and cannot finish three-dimensional structures or curved surfaces.

In this study, after EDM, the PCD electrode was used directly as a grinding wheel for finishing the EDMed surface and removing the SSD layer. Because the metallic binder in PCD is preferentially removed by electrical discharges during EDM, diamond grains protrude out of the PCD surface and act as fixed abrasive cutting edges, which remove the SSD layers efficiently through ductile mode grinding, as shown in Fig. 1b. The proposed machining

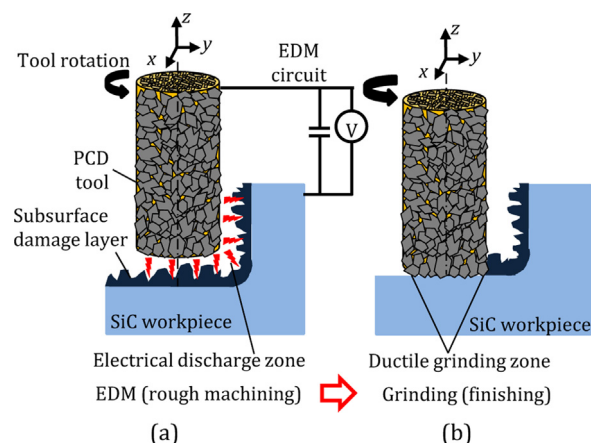


Fig. 1. Models for micromachining of SiC using a PCD hybrid tool.

* Corresponding author.

E-mail address: yan@mech.keio.ac.jp (J. Yan).

process uses a single tool on a single machine, and takes advantage of both the high MRR of EDM and the high surface integrity of grinding. In addition, it enables the flexible machining of three-dimensional and curved structures.

3. Experimental procedures

PCD rods, containing diamond grains with a mean size of $0.5\ \mu\text{m}$ at a concentration of 90% in a Co binder, with diameters of 1 mm were used as tools. The thermal conductivity of PCD is $290\ \text{W}/(\text{m K})$. An *n*-type single-crystal 4H-SiC wafer with a surface orientation of (0 0 0 1) was used as the workpiece. The wafer was 50 mm in diameter and 0.36 mm in thickness, with a CMP finish. 4H-SiC has a hexagonal structure with lattice constants of $a = 3.073\ \text{\AA}$ and $c = 10.053\ \text{\AA}$. It has a Mohs hardness of 9, thermal conductivity of $370\ \text{W}/(\text{m K})$, melting point of $2730\ ^\circ\text{C}$, sublimation point of $2830\ ^\circ\text{C}$, relative dielectric constant of 9.76, band gap of 3.26 eV, and electrical resistivity ranging from 13.0–25.0 $\text{m}\Omega\ \text{cm}$.

A micro-EDM machine (Panasonic MG-ED82 W) was used in the experiments. The *xyz*-axes tables of the machine have a stepping resolution of $0.1\ \mu\text{m}$, and the feeding speed of the tool electrode is controlled automatically by the machine controller. The machine is powered by a resistor–capacitor (RC) pulse generator, where the electrical capacitance varies from 3300 to 100 pF. EDM experiments were performed at voltages of 70 and 110 V, using PCD as anode and SiC as cathode. The tool electrode's rotation rate was 3000 rpm.

Both plunge grinding and mill grinding were performed using the same EDM machine and the same PCD tool. In plunge grinding, the tool feed rate in the *z* direction was $0.1\ \mu\text{m}/\text{s}$. In mill grinding, the depth of cut in the *z* direction per tool pass was $1\ \mu\text{m}$ and the tool feed rate in the *y* direction was set between 2.5 and $25\ \mu\text{m}/\text{s}$. The total depth of grinding was $10\ \mu\text{m}$.

4. Results of micro-EDM

4.1. Surface topography

The effects of discharge energy on the workpiece's surface topography were investigated. Fig. 2 shows SEM images of EDMed surfaces at voltages of 70 and 110 V and a capacitance of 3300 pF. The surfaces are roughened by craters. As voltage increased from 70 to 110 V, the size and depth of craters also increased, creating an increase in surface roughness R_a from 0.368 to $0.417\ \mu\text{m}$.

4.2. Subsurface material structure

Fig. 3 shows cross-sectional SEM images of the EDMed surfaces, corresponding to those in Fig. 2. At the top of each surface, thick recast layers are clearly seen. As voltage increases from 70 to 110 V, the thickness of the recast layer increases from ~ 2 to $\sim 3\ \mu\text{m}$. The results strongly demonstrate that 4H-SiC undergoes melting and resolidification during EDM, and that the local temperature in the electrical discharge zone rises above $2730\ ^\circ\text{C}$, the melting point of 4H-SiC.

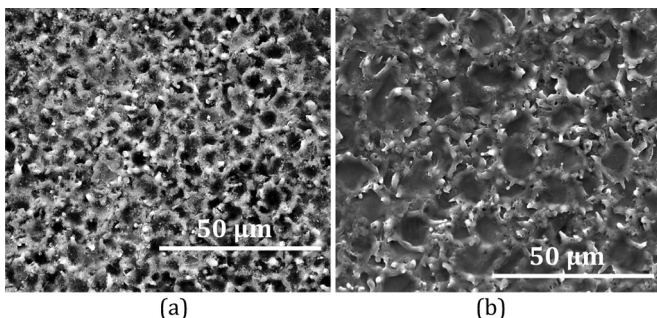


Fig. 2. SEM images of EDMed SiC surfaces at (a) 70 V and (b) 110 V, showing an increase in surface crater size and depth with voltage.

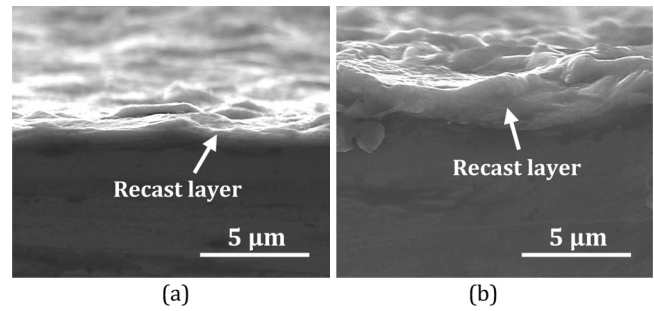


Fig. 3. Cross-sectional SEM images of EDMed surfaces at (a) 70 V and (b) 110 V, showing an increase in recast layer thickness with voltage.

4.3. Raman spectroscopy and nanoindentation hardness

To detect possible structural changes of material in the recast layers, laser Raman spectroscopy was performed before and after EDM. Fig. 4a and b show Raman spectra of the pristine SiC wafer and the EDMed surface shown in Fig. 2a, respectively. In Fig. 4a, three typical Raman peaks of SiC are clearly identified. In Fig. 4b, however, a few new peaks appear. The two broad peaks at 1590.65 and $1347.98\ \text{cm}^{-1}$ indicate the presence of graphite, a C allotrope, and the sharp peak at $520.19\ \text{cm}^{-1}$ demonstrates the existence of crystalline Si. Although the C component maybe partially from the decomposition of dielectric oil, the presence of Si indicates that SiC decomposed into Si and C during EDM. Owing to this material decomposition, the recast layer is significantly softer than the bulk. We measured the hardness of the sample using nanoindentation and found that the hardness of the recast layer was $1.97 \times 10^4\ \text{N}/\text{mm}^2$, significantly lower than that of the pristine SiC wafer ($3.52 \times 10^4\ \text{N}/\text{mm}^2$).

Fig. 5a shows a schematic of material removal in EDM. The high temperature generated in the electrical discharge zone [12] causes melting and vaporization of the worked material, leaving craters

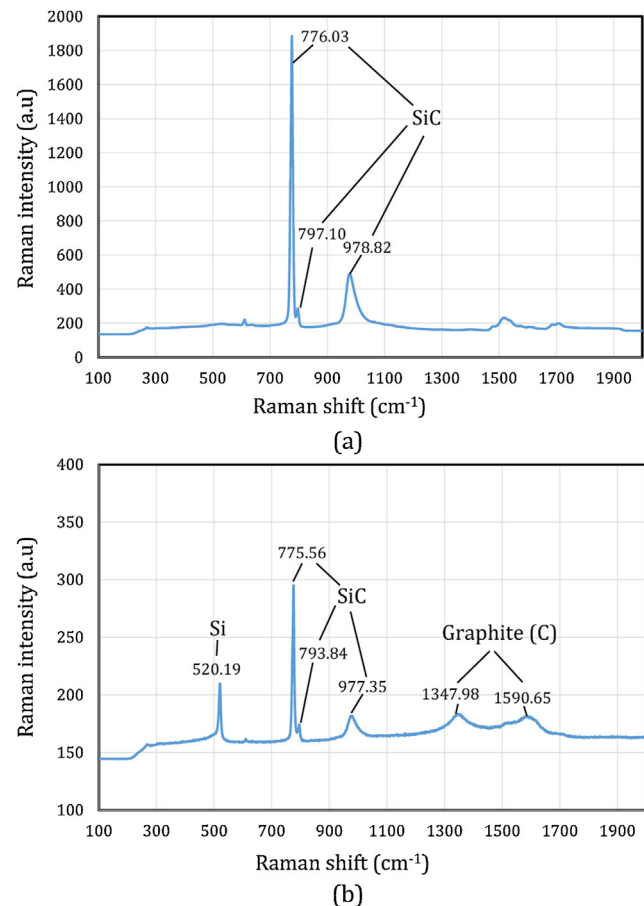


Fig. 4. Raman spectra of the SiC wafer (a) before EDM and (b) after EDM.

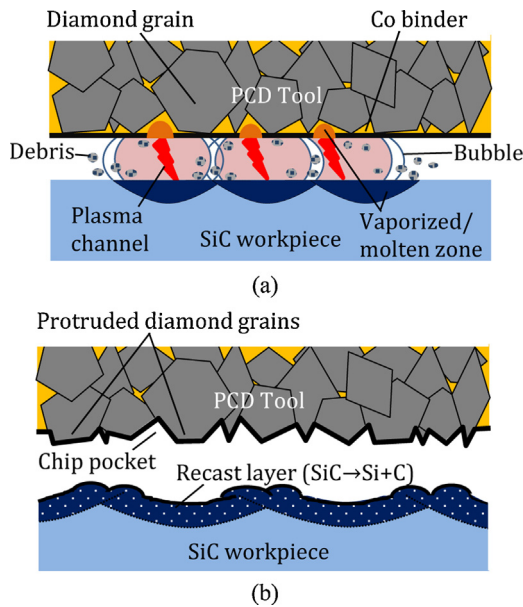


Fig. 5. Schematics of (a) material removal in EDM and (b) topographical and structural changes in both PCD and SiC.

on the workpiece surface. Fig. 5b shows topographical changes of PCD and structural changes in SiC after EDM. Owing to the material decomposition of SiC, the workpiece undergoes surface softening. Meanwhile, the Co binder on the PCD tool surface is preferentially removed during EDM, creating chip pockets and permitting diamond grains to protrude out of the tool’s surface, similar to the electrical discharge dressing of grinding wheels. These two aspects, namely, workpiece surface softening and diamond grain protrusion, are essential for the subsequent ductile mode grinding process.

5. Results of micro-grinding

5.1. Surface topography change

With the EDM power source switched off, the same PCD tool was used directly for plunge grinding tests in the SiC sample. A cut depth of 10 μm was defined in the z direction with no tool feed in the y direction. Fig. 6 shows SEM images of the bottoms (a, c) and

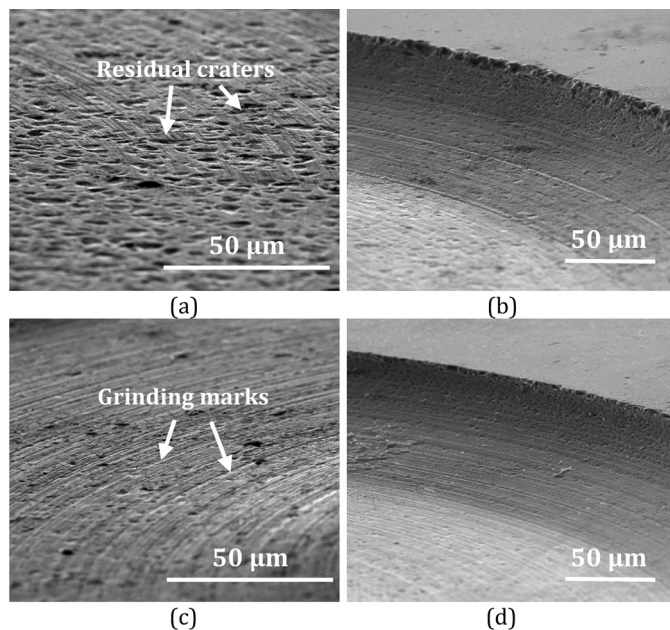


Fig. 6. SEM images of the bottoms (a, c) and fringes (b, d) of EDMed cavities after plunge grinding. The voltages used in EDM were (a, b) 110 V and (c, d) 70 V.

fringes (b, d) of two EDMed cavities. For the cavity EDMed at a voltage of 110 V (a, b), discharge craters were not completely removed by grinding, indicating that the SSD was deeper than 10 μm. For the cavity EDMed at 70 V (c, d), however, craters are barely visible, with only grinding marks evident on the surface.

5.2. Raman spectroscopy analysis

Fig. 7 shows the Raman spectrum of the ground surface shown in Fig. 6c; it is very similar to that in Fig. 4a. The Raman peaks indicating C and Si, shown in Fig. 4b, do not appear in Fig. 7, demonstrating that the recast layer has been removed by grinding. Therefore, by using a depth of cut greater than the sum of crater depth and recast layer thickness, it is possible to completely remove the EDM-induced recast layer by grinding. It should be noted that grinding itself may cause SSD, such as dislocation and residual stress, but it is insignificant and difficult to detect by Raman spectroscopy.

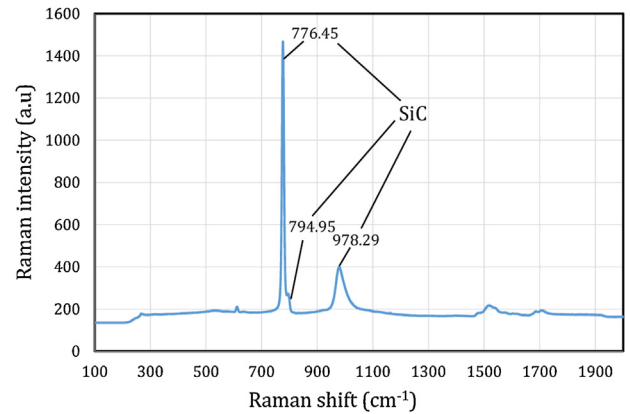


Fig. 7. Raman spectra of the workpiece surface after grinding, showing a typical SiC structure without Si or C allotropes.

5.3. Tool surface topographical change

Fig. 8 shows SEM images of a PCD tool surface before and after grinding. In Fig. 8a, aggregations of diamond grains protrude from the tool surface, and chip pockets were formed during EDM. After grinding, the diamond grain aggregations have been slightly flattened and material adhesion was found on the tool surface, as seen in Fig. 8b. Energy dispersive X-ray spectrometry (EDX) analysis showed that the adhered material was mainly Si, which was removed from the recast layer of the SiC workpiece by ductile mode grinding.

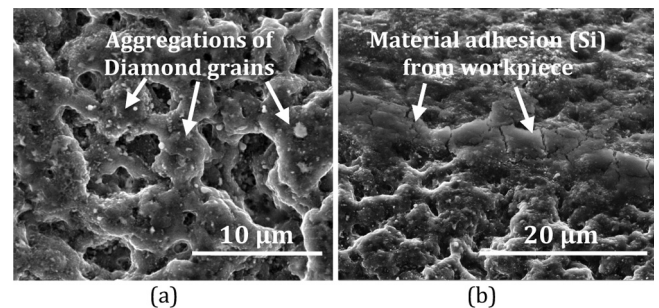


Fig. 8. SEM images of the surface of the PCD tool (a) after EDM and (b) after grinding.

5.4. Effects of transverse tool feed

To eliminate the grinding marks formed via plunge grinding, as shown in Fig. 6, mill grinding was performed by traverse feeding the PCD tool in the y direction. Fig. 9a is a micrograph of an EDMed micro-cavity. The surface is rough with dense discharge craters. Fig. 9b shows an EDMed and then mill-ground micro-cavity at a

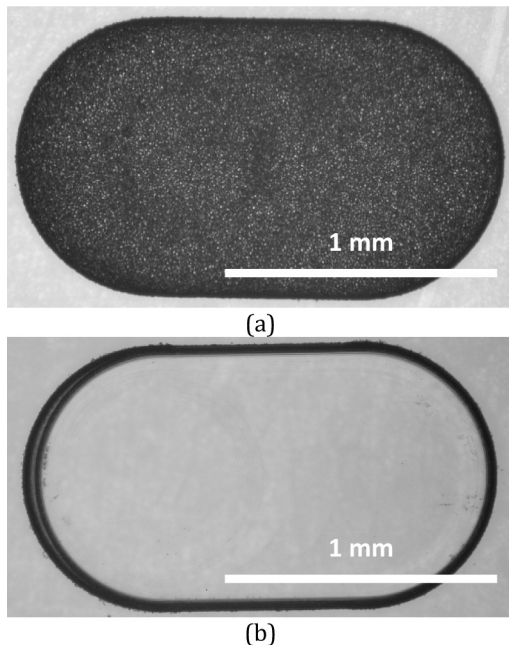


Fig. 9. Micrographs of (a) an EDMed cavity and (b) an EDMed and then mill-ground cavity by introducing a traverse tool feed.

traverse tool feed rate of 25 $\mu\text{m/s}$. The surface appears as smooth as the surrounding area finished by CMP. The time for EDM was 8.1 min and that for grinding was 7.3 min, respectively.

Fig. 10 shows three-dimensional topographies of the bottom surfaces of the cavities shown in Fig. 9, which were measured using a white light interferometer; Fig. 11 shows a plot of surface roughness after different process steps. The surface roughness of

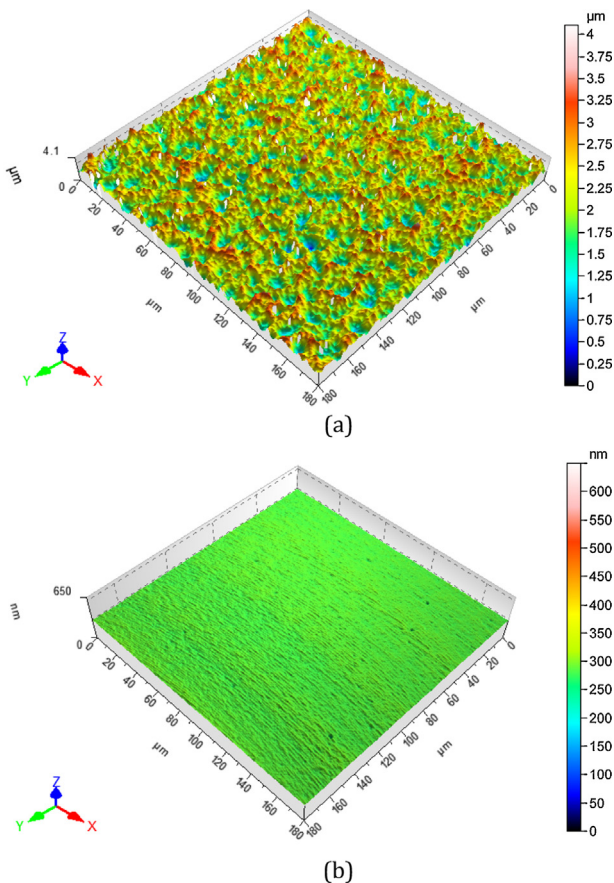


Fig. 10. Three-dimensional topographies of the bottom surfaces of the cavities shown in Fig. 9, (a) without and (b) with grinding.

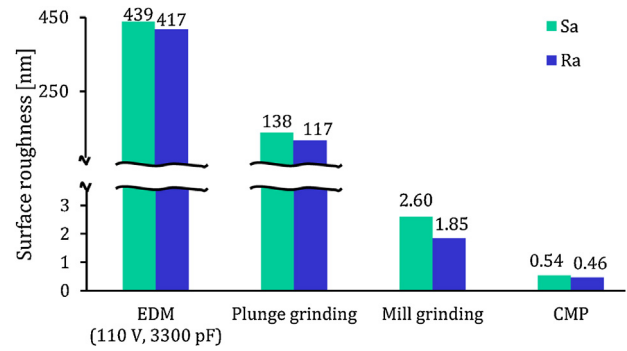


Fig. 11. Comparison of surface roughness resulting from different process steps using the PCD hybrid tool versus CMP.

an as-received 4H-SiC wafer with a CMP finish is also shown for comparison. The surface roughness R_a after EDM was 417 nm ($S_a = 439$ nm). After mill grinding, however, R_a decreased to 1.85 nm ($S_a = 2.60$ nm), a factor of 200 less than that of the EDMed surface. The surface quality resulting from the proposed process approaches that achieved by CMP, while the processing time is distinctly shorter than that of CMP.

As a future task, the effects of other process factors, such as tool geometry, mean size and concentration of diamond grains in PCD, as well as EDM conditions will be further investigated.

6. Conclusions

PCD was used as a hybrid tool for micro-scale EDM and grinding of single-crystal SiC. EDM created a thick recast layer where SiC decomposed into C and Si, leading to significant surface softening. During EDM, diamond grains began to protrude out of the PCD tool surface by the electrical discharge dressing effect, which greatly improved the tool's subsequent ductile grinding performance. Mill grinding after EDM using the hybrid tool with a traverse tool feed enabled complete removal of the EDM-induced recast layer with a nanometer-scale surface finish ($R_a = 1.85$ nm).

References

- [1] Tanaka H, Shimada S (2013) Damage-Free Machining of Monocrystalline Silicon Carbide. *CIRP Annals* 62(1):55–58.
- [2] Zhao Y, Kunieda M, Abe K (2013) Experimental Investigations into EDM Behaviors of Single Crystal Silicon Carbide. *Procedia CIRP* 6:135–139.
- [3] Kimura A, Okamoto Y, Okada A, Ohya J, Yamauchi T (2013) Fundamental Study on Multi-wire EDM Slicing of SiC by Wire Electrode with Track-shaped Section. *Procedia CIRP* 6:232–237.
- [4] Kitamura T, Kunieda M (2014) Clarification of EDM Gap Phenomena Using Transparent Electrodes. *CIRP Annals* 63(1):213–216.
- [5] Nakaoku H, Masuzawa T, Fujino M (2007) Micro-EDM of Sintered Diamond. *Journal of Materials Processing Technology* 187–188:274–278.
- [6] Zhang Z, Peng H, Yan J (2013) Micro-Cutting Characteristics of EDM Fabricated High-Precision Polycrystalline Diamond Tools. *International Journal of Machine Tools and Manufacture* 65:99–106.
- [7] Yan J, Watanabe K, Aoyama T (2014) Micro-Electrical Discharge Machining of Polycrystalline Diamond Using Rotary Cupronickel Electrode. *CIRP Annals* 63(1):209–212.
- [8] Katahira K, Takesue S, Komotori J, Yamazaki K (2014) Micromilling Characteristics and Electrochemically Assisted Reconditioning of Polycrystalline Diamond Tool Surfaces for Ultra-precision Machining of High-Purity SiC. *CIRP Annals* 63(1):329–332.
- [9] Suzuki K, Sharma A, Sano S, Iwai M, Uematsu T (2005) A New Application of PCD as a Very Low Wear Electrode Material for EDM. *Key Engineering Materials* 291–292:549–554.
- [10] Uhlmann E, Roehner M (2008) Investigations on Reduction of Tool Electrode Wear in Micro-EDM Using Novel Electrode Materials. *CIRP Journal of Manufacturing Science and Technology* 1(2):92–96.
- [11] Yamamura K, Takiguchi T, Ueda M, Deng H, Hattori AN, Zettsu N (2011) Plasma Assisted Polishing of Single Crystal SiC for Obtaining Atomically Flat Strain-Free Surface. *CIRP Annals* 60(1):571–574.
- [12] Hinduja S, Kunieda M (2013) Modelling of ECM and EDM Processes. *CIRP Annals* 62(2):775–797.